Investigation of Radar-Based Gait Measurement in a Simulated Home Environment With a Microwave CW Radar

Master's thesis in Master Biomedical Engineering

ALEXANDER SUNDVALL

Department of Electrical Engineering
CHALMERS UNIVERSITY OF TECHNOLOGY
Gothenburg, Sweden 2022

MASTER'S THESIS 2022:EENX30

Investigation of Radar-Based Gait Measurement in a Simulated Home Environment With a Microwave CW Radar

ALEXANDER SUNDVALL

Department Electrical Engineering
Division of Signal Processing and Biomedical Engineering
CHALMERS UNIVERSITY OF THECHNOLOGY
Gothenburg, Sweden 2022

Investigation of Radar-Based Gait Measurement in a Simulated Home Environment With a Microwave Cw Radar

Alexander Sundvall

Supervisor: Xuezhi Zeng, Signals and systems
Examiner: Xuezhi Zeng, Signals and systems

Master's Thesis 2022:EENX30
Department of Electrical Engineering
Division of Signal Processing and Biomedical Engineering
Biomedical electromagnetics group
Chalmers University of Technology
SE-412 96 Gothenburg
Telephone +46 31 772 1000

Gothenburg, Sweden 2022

Investigation of Radar-Based Gait Measurement in a Simulated Home Environment With a Microwave CW Radar
Alexander Sundvall
Department of Electrical Engineering
Chalmers University of Technology

Abstract

In this thesis, a gait measurement system using a continuous wave (CW) microwave radar was developed. The aim was to investigate the reliability of the system in the estimation of gait parameters in a simulated home environment where clutter was present, relative to an ideal environment without any clutter present. A total of 87 measurements were taken with four different gait patterns considered: slow pace, medium pace, fast pace, and limping. The tests were performed in three different measurement scenarios: one being an ideal environment without any clutter and the other two being a simulated home environment with a clear and obstructed line of sight. In total six gait parameters were extracted from the measurement data and these parameters were validated using video recordings. The results indicate that the presence of clutter has a very minor impact on the accuracy of the estimated parameters relative to the system accuracy in the ideal environment, and that the accuracy of the estimated gait parameters is instead far more dependent on the quality of the measurements and the accuracy of the system.

Keywords: Doppler radar, Gait analysis, Signal processing

Acknowledgements

I want to begin by expressing my gratitude and appreciation to my supervisor Xuezhi Zeng for offering her assistance and insight during the course of the project whenever I needed it, and for reading and providing feedback to the many drafts of the thesis. I would not have been able to complete this thesis without her guidance.

I also want to thank Halldór Stefán Laxdal Báruson, who was working on a similar thesis at the same time. I wish to thank him for his aid in the collection of radar measurements by taking on the role of walking in front of the radar, and for being willing to discuss and compare our different ideas and methods.

Lastly I would like to give special thanks my parents for their constant support and motivation over the years, without them it would not have been possible to come as far as I have.

Contents

List of Figures

List of Tables

Chapter 1

Introduction

This chapter introduces the application of radar for the purpose of gait measurement within a home environment is introduced, along with a background of the subject and the existing methods for measuring gait. The chapter concludes with the project aim and an outline of the thesis.

1.1 Background

The worlds population of elderly adults over the age of 60 has been growing steady for over a century [1, 2], and is predicted to reach a size that is 50% of the population of adults over the age of 20 by the year 2050 [1]. This means that there is a growing set of people that suffer from a variety of health conditions that are related to ageing, including conditions that affect a persons cognitive state. These include neurodegenerative disorders such as Parkinson's disease, which is the second most common age-related neurodegenerative disorder after Alzheimer's disease and is estimated to cost nearly $52 billion per year in the USA [3, 4]. This population also suffer from an increased fall risk, with more than one in four adults over the age of 65 falling each year [5, 6]. Falls are the leading cause of death for that same age group and in the USA the total medical cost for falls is over $50 billion [6, 7]. If these conditions could be detected and diagnosed in their early stages then the onset of these conditions could be delayed, or in some cases prevented, by implementing the appropriate early intervention. [3, 8, 5].

The conditions that are mentioned above are among other things characterized by impairments in the gait, which refers to the movement pattern of a persons body and limbs that they adopt as they are walking [3, 5]. For example, the gait of people with Parkinson's disease tends to be shuffling with small steps [3]. It has been shown that in order for gait to be safe and effective it requires input from higher cognitive ares, and that these areas overlap with other cognitive domains such as executive function and memory [3, 8, 9, 5, 10]. This means that any conditions that would cause impairments in any of these cognitive domains would also manifest as impairments in the gait [9]. Thus by monitoring the gait of elderly adults over time for early changes would enable the prediction and diagnosis of future cognitive impairments. However, these early changes are too subtle to be detected by the human eye and thus a more detailed assessment is required which is usually performed using specialized equipment in a gait lab [9, 5, 7]. The measurements performed in gait labs are very accurate but are also costly, time consuming, and require the support of trained personal to operate the equipment [8, 7]. Additionally, a persons gait changes when their full attention is dedicated to it compared to their natural gait, which is why gait tests are often preformed as dual-task tests where a simple task such as counting is performed in conjunction with walking [5, 7, 11]. The gait must also be measured very frequently in order to detect the long term changes that would be used to assess and predict cognitive impairments. Thus, due to the resource demand of gait labs and the measurement frequency requirement for detecting the early changes in the gait, it would be unfeasible to monitor the gait of every elderly through the use of gait labs. It would be far more practical to install a system within the home that could then continuously monitor the gait of the inhabitant. This would then allow the elderly to remain within their homes for a longer time, which is something that many desire to do [1]. There is thus a need for a system that can be deployed within a home environment and is able to measure and asses the gait of the inhabitant.

1.2 Existing methods for measuring gait

Many different types of systems have been investigated for the purpose of in-home gait measurement, which can broadly be divided into wearable and non-wearable systems [12, 13]. The wearable systems measure the gait of the subject though several sensors, for example accelerometers, that are each attached to specific locations on the body, such as feet, knees, etc. [7, 13, 14]. These types of systems have been shown to be very accurate but suffer from certain drawbacks that make them inadequate as in-home gait monitoring systems [7, 12, 13, 15]. One major drawback is that these systems depend on the subject's continued remembrance and cooperation regarding the attachment of the sensors, and that they attach them correctly [7, 12, 13, 15]. Some other drawbacks are that they could be destroyed if dropped or sat on, they have a short battery life, and that their presence on the body could potentially affect the gait [7, 12, 15].

The non-wearable systems measure the gait of the subject using sensing technologies that are not attached to the body. These types of systems include in-ground force platforms and camera-based systems operating at visible or infrared light [7, 12, 14, 16]. The benefit of these types of systems over wearable systems is that they are able to measure the gait without the attention or cooperation of the subject. However, they have their own drawbacks as well. The in-ground force platforms have a range that is limited to their own surface and would be cumbersome to install [8], while the camera-based systems provide better coverage than the platforms but are still limited to single rooms and would thus require several cameras to cover a home [13]. In addition, the infrared cameras often require that their entire body is within the field of view and the video cameras are easily affected by poor lighting conditions, occlusions, and clothing [8, 7, 12, 16]. The camera systems also suffer from perceived privacy concerns as many people are uncomfortable with being constantly monitored in their home [12, 15, 17].

1.3 Radar for gait measurement

In recent years, radar systems have been gaining more attention as a more preferable alternative as an in-home gait monitoring system [8, 12, 13, 16, 18]. This is because radar systems provide the same benefits as non-wearable systems, along with being privacy preserving and being able to operate effectively without being affected by lighting, occlusions, or clothing [8, 13, 17, 18, 19]. These systems measure the gait by analysing the small, time-varying Doppler-shifts in the return signal that are caused by the movement of the subjects body and limbs, referred to as micro-Doppler signatures [13, 17, 18, 20]. Several different types of radar systems have been investigated for this purpose across many studies. As examples, these include the following works; Saho et al. used a continuous wave (CW) radar to extract certain velocity parameters from the micro-Doppler signatures and investigated their associations with the cognitive functions of the elderly [8]. Seifert et al. were able to reliably extract five spaciotemporal parameters and three kinematic paramenters from the micro-Doppler signatures using a ultra wide-band (UWB) radar [12]. Wang et al. were successful in extracting some gait parameters such as torso velocity and step time using a pulse-Doppler radar [7]. However, the majority of previous studies that have investigated and validated radar-based gait measurement, including those mentioned above, have only preformed their experiments under ideal conditions within a lab. In these studies the subjects walked toward and away from the radar without any other objects that could cause interference present in the space. Very few studies have actually tested their systems reliability within a home environment [21], even among those that are specifically concerned with in-home gait analysis [7, 16, 17].

1.4 Aim

The aim of this thesis is to develop a radar-based gait measurement system and investigate its efficacy and reliability as a continuous monitoring system within a home environment. The main objectives of this thesis include:

- Develop a system that is able to detect the return signal from the target and extract the micro-Doppler signatures from that signal.
- Determine the reliability of the system when the monitored space contain stationary objects commonly found in home environments, such as tables, chairs, etc.
- Investigate strategies to improve the reliability of the system by employing different signal processing techniques.
- Suggest additional features and improvements upon the system that would enhance the performance of the system which could be the subject of future works.

1.5 Thesis outline

This thesis has the following outline: Chapter 1 provides an introduction to the topic and describes the aim of the thesis. Chapter 2 describes the theory behind radar measurements using CW radar, along with the data structures that are computed from the radar return signal. Chapter 3 describes the equipment and software used in this thesis, how the measurement data is processed in order to extract the gait parameters, and what tests are performed to validate the developed system. Section 4 presents the results of the tests. In Chapter 5, the results from the tests are discussed along with data that was not included in the results and possible sources of error. Chapter 6 presents the conclusion of the thesis.

Chapter 2

Theory

This chapter begins with a description of how human gait is modeled and how gait is related to cognition. It then presents the underlying theory behind radar measurements using CW radar, followed by the data representations that are used for extracting the gait parameters from the measurement data. The chapter concludes with a basic introduction to the Wavelet transform and its application in data denoising.

2.1 Gait and its relation to cognition

In order to analyse the movement pattern that is human gait it is modeled as a set of spatial, temporal, and velocity parameters. Due to the periodic nature of the gait, these parameters are all characterized by the heel-strikes and toe-offs that occur within a single gait cycle, which is defined between the heel-strike of either foot to the next heel-strike of the same foot [12]. The heel-strike occurs when the heel first makes contact with the ground while the toe-off occurs when the toes just loses contact with the ground. Two consecutive heel-strikes of opposite feet defines a step while two consecutive heel-strikes of the same foot defines a stride. This means that a single gait cycle contains the occurrence of two steps or one stride. Figure 2.1 illustrates how the spatial and temporal parameters are defined in the gait cycle [5, 11]. Regarding the spatial parameters, the step length is the distance covered by a single step [12], the stride length is the distance covered by a stride [12], and the step width is the normal distance between steps. Regarding the temporal parameters, the step time is the time period for a single step [12], the stance time is the duration where the foot is in contact with the ground [12], the swing time is the duration where the foot is traveling through space [12], and the stride time is the duration of a stride [12]. The velocity parameters include the step velocity which is the maximal velocity achieved by the foot during a step [12]. Since a human does not walk with perfect consistency, the parameters are given by the mean over multiple steps while the variability of the parameters are given as the standard deviation of the measurements [11]. The asymmetry of the spatio-temporal parameters relating to the steps (Step time, Step length, Stance time, Swing time) can also be determined as the mean difference between the two steps of a gait cycle.

The gait of a human can be further modeled by grouping parameters into gait domains. One such

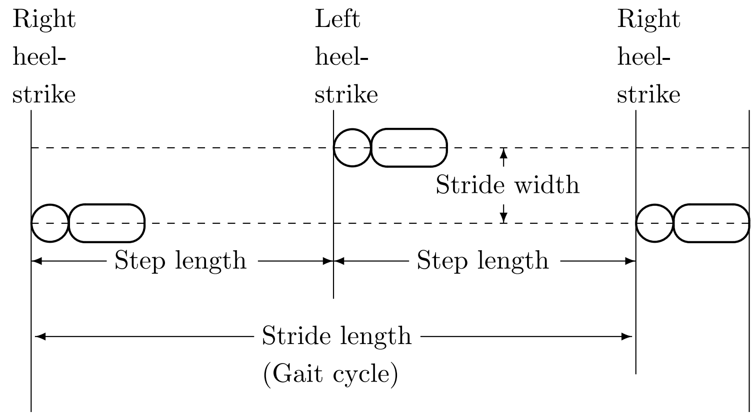

(a) Definition of the spatial gait parameters based on the placement of the feet

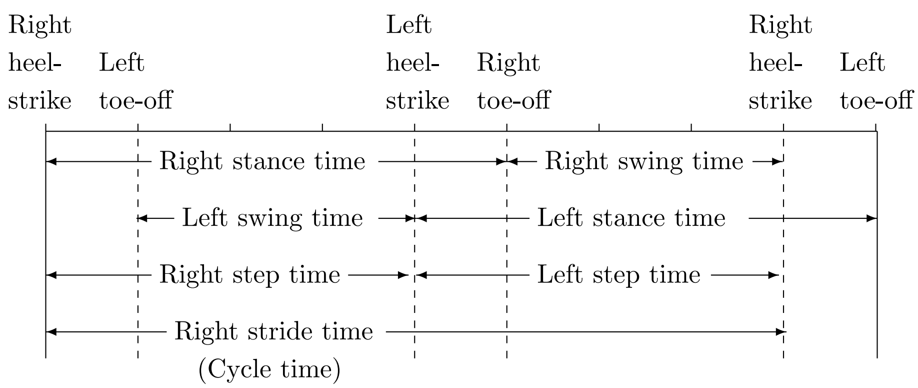

(b) Definition of the temporal gait parameters based on the instances of the heel-strikes and toe-offs

Figure 2.1: Diagram illustrating the definition of the spatio-temporal gait parameters

model with the domains Pace, Rhythm, Variability, Asymmetry, and Postural control is presented in Table 2.1, along with the associated parameters and their units [10]. As mentioned in Section 1.1, it has been shown that gait requires input from higher cognitive domains and that these domains overlap with other cognitive domains such as those associated with executive attention and memory [3, 8, 9, 5, 10]. Thus any pathology that would cause impairments in these cognitive domains would also cause the gait to change accordingly. However, the different aspects of the gait are not all connected to the same cognitive domains, and since the cognitive domains are affected differently depending on the pathology the changes in the gait manifest in different gait domains [10]. For example, changes in the Pace domain was predictive of decline in executive function [9, 10], changes in the Rhythm domain was predictive of decline in memory [9, 10], and changes in the Variability domain was predictive of an increased risk of falling [9].

Table 2.1: Table of some gait parameters, the associated gait domains, and the units of each parameter

Gait domain	Parameter	Unit
Pace	Step velocity	m/s
	Step length	m
	Step time variability	ms
	Step swing time variability	ms
	Step stance time variability	ms
Rhythm	Step time	ms
	Step swing time	ms
	Step stance time	ms
Variability	Step velocity variability	m/s
	Step length variability	m
	Step width variability	m
Asymmetry	Step time asymmetry	ms
	Step swing time asymmetry	ms
	Step stance time asymmetry	ms
Postural control	Step width	m
	Step length asymmetry	m

2.2 The principle of CW Doppler radar

The way that CW Doppler radar systems performs measurements is by transmitting a single frequency signal continuously for the entire duration of the measurement [22]. This means that these systems cannot determine the range of the target and are thus only able to measure the relative displacement of the target through the Doppler effect [22]. Due to this lack of range information it also means that this type of radar is incapable of distinguishing between different targets, so it is only suited for monitoring a single person. However this also means that it becomes simpler to process the data since the frequency contents of the return signal will only contain frequencies caused by the relative displacement of the target, with the addition of some noise.

The signal that is transmitted by the system $s_t(t)$ is given by [16, 19]

$$s_t(t) = A\,cos(2\pi f_c t) \tag{2.1}$$

where f_c is the carrier frequency of the signal and A is the amplitude. When this signal illuminates a person, the movements of the limbs and body will cause a frequency shift in the scattered signal in accordance with the Doppler effect [16, 17, 19, 20]. Since the various body parts move at different velocities they will cause different frequency shifts, which are referred to as Doppler shifts or Doppler frequencies, turning the return signal into a superposition of frequency modulations that will vary with time, which are the previously mentioned micro-Doppler signatures [16, 19, 17, 20]. The return signal $s_r(t)$ can then be represented as [16, 19]

$$s_r(t) = \sum_i \rho_i cos(2\pi(f_c + f_i^D)t) \tag{2.2}$$

where ρ_i is the path loss of the scatter component from the ith body part and f_i^D is the Doppler shift caused by that body part. When the return signal is detected at the receiver it is then down-converted into its baseband representation, which is expressed as [16]:

$$s(t) = \sum_i \frac{\rho_i}{2} e^{-j2\pi f_i^D t} \tag{2.3}$$

The remaining frequency contents of the signal will thus only consist of the micro-Doppler signatures which can be used to estimate the velocities of the moving body parts by utilizing the relationship [16]

$$f_i^D \approx f_c \frac{2v_i(t)}{c} = \frac{2v_i(t)}{\lambda_c} \tag{2.4}$$

where $v_i(t)$ is the Doppler velocity that generated the ith Doppler shift and c is the speed of light. By rearranging this equation the Doppler velocity of the ith body part can be calculated from the corresponding Doppler shifts as

$$v_i(t) \approx \frac{f_i^D \lambda_c}{2} \tag{2.5}$$

2.3 Data representation of gait

Since the micro-Doppler signatures are frequency modulations within the signal, the frequency contents must be analysed in order to extract them. The usual method for this kind of analysis is to apply the Fourier transform (FT) to the signal [16, 19]. However, the FT represents the frequency contents of the signal for the entire duration and thus loses any sense of time-localization, i.e are the previously mentioned micro-Doppler signatures [7, 16, 19]. This aspect of the FT makes it unsuitable for analysing the micro-Doppler signatures since they very localized in time. Thus, in order to capture the time-varying nature of the signatures they must be analysed using a joint time-frequency representation (TFR), which depicts the frequency behavior of the signal that is local in time [16, 17, 19]. The most common TFR is the Spectrogram which is the squared magnitude, and thus the energy, of the Short-Time Fourier Transform (STFT) [16, 17, 19]. The STFT is an intuitive solution to circumvent the lack of time-localization in the FT, which involves applying a sliding window function to the signal and then computing the FT of the windowed signal [19]. The sample offset between each successive window determines the time resolution of the STFT, while the frequency resolution of the STFT is determined by the length of the window function since the frequency resolution of the FT is related to the inverse of the time duration of the signal it is applied to. Thus a small window will provide a fine time-localization but a coarse frequency resolution, and vice versa for a large window. This must be taken into account when choosing the size of the window so that the frequency contents of the signal are properly resolved while maintaining a good time-localization. The Spectrogram is computed as [7, 16]

$$S(n,k) = \left| \sum_{m=0}^{M-1} w(m)s(n+m)e^{-j2\pi mk/K} \right|^2 \tag{2.6}$$

where w is the sliding window, $m = 0, 1, ..., M-1$ is the sample index of the window, M is the length of the window, s is the signal, $n = 0, 1, ...N-1$ is the sample index of the signal, $k = 0, 1, ...K-1$

is the frequency index. The horizontal axis of the Spectrogram correspond to time and the vertical axis correspond to Doppler frequency. The Spectrogram can be used to compute the envelopes of each moving body part, i.e torso, knee, foot. The envelope of a body part is a time domain signal that encapsulates the Doppler frequencies from the micro-Doppler signatures that are caused by that body part, which can be used to determine the velocity profile of the body part after the envelope is converted to velocity according to equation (2.4).

From the Spectrogram another data structure is derived called the Cadence Velocity Diagram (CVD) [16, 20], which is computed by taking the FT of each discrete Doppler frequency in the Spectrogram. This preserves the vertical axis as the Doppler frequency while transforming the horizontal axis into the frequency domain [16, 20], referred to as the Doppler repetition frequency. Thus, the CVD represents the repetition frequency of certain Doppler shifts, which better enables the analysis of the periodic patterns that are inherent to human gait, such as the torso velocity, the average velocity of the body, and the cadence, the number of steps per second. The torso velocity is related to the Doppler frequency with the highest energy in the CVD, because the torso reflects the most amount of energy, which will be very close to the DC component of the Doppler repetition frequency since the torso motion is almost constant and thus causes very low oscillation in the Doppler shift. For a similar reason, the cadence is related to the fundamental frequency of the Doppler repetition frequency in the case of unaided gait i.e. no cane, because the leg motion reflect the most amount of energy, and has the most prominent oscillation in the Doppler shifts, after the torso. The reason for the CVD being a better method for analysing the periodic patterns of the gait is because representation of these patterns in the CVD is time-invariant, which means that it is not dependent on where in the gait cycle that the measurement begins and ends [16]. Contrast this with, for example, determining the cadence using the Spectrogram which is completely dependent on the correct identification of the number of steps present within the measurement, which will necessitate the identification of partial steps since the measurement window is unlikely to perfectly align with the gait cycles, and it is also unlikely that the cadence of the target would perfectly fit an integer number of steps within the measurement. The CVD is computed as [16, 20]

$$C(l,k) = \left| \sum_{n=0}^{N-1} S(n,k) e^{-j2\pi nl/L} \right| \tag{2.7}$$

where $l = 0, 1, ..., L-1$ is the index of the Doppler repetition frequency and the other are the same as those from the computation of the Spectrogram in equation 2.6.

2.4 Basics of the Wavelet transform

In this project the Wavelet transform was used to denoise the measurement data, and thus a very basic explanation of the underlying theory behind the Wavelet transform and its application in data denoising is presented in this section.

The Wavelet transform is a method for analysing the frequency contents of a signal that depicts the dominant frequencies of the signal at different time scales [23], and has applications in image compression and in signal processing, which includes the denoising of data [23]. The transform provides an adaptive time-frequency resolution in the sense that it has a constant relative bandwidth, which is what enables it to depict the frequency content of the signal at different time scales. This means that the small-scale features of the signal are analysed using a fine time resolution and a coarse frequency resolution while the reverse is used to analyse the large-scale features [23]. By contrast, the STFT has a constant time-frequency resolution because the analysis is carried out using a sliding window of constant size, and is thus locked to a single time scale.

The first step in the transformation is to apply two sliding filters to the data, the wavelet function and the corresponding scaling function, which essentially operates as a high-pass and low-pass filter respectively [23]. This results in two separate data sets, where one contain coefficients that represents the features on the smallest scale while the other contain coefficients that represents an approximation of the data, which can be thought of as high-passed and low-passed versions of the data [23]. The two filtered data sets are then downsampled by a factor of two which is done in order to avoid redundancy [23]. Performing this step would cause aliasing if applied to the Fourier transform but the filters used in the previous step are constructed in such a way that it does not occur [23]. This procedure is then repeated for the desired number of iterations, with the approximation, or the "low-passed" data, now considered as the new input data [23]. The resulting data set has the same size as the original data, and is composed of a number of coefficients that represent a coarse approximation of the data and then a sequence of finer and finer details [23]. An example of the transform procedure is illustrated in Figure 2.2 where three iterations are used, and the symbols A_i and D_i correspond to the coarse approximation and the details of each level of data decomposition within the transform. The inverse transform is basically the reverse of the iterative process where the approximation and the coarsest details are upsampled, filtered, and added together [23]. This process is then repeated for the same number of iterations as was used in the original transform.

The adaptive time-frequency resolution, and the non-redundancy of the Wavelet transform, results in a very important property: the majority of the information that is contained in the data is concentrated into a few large Wavelet coefficients, while the noise is spread out over many small coefficients [23]. It is this property that makes the Wavelet transform so useful for data denoising, because by identifying the small coefficients within each set of details in the transform using a threshold and then setting the small coefficients to zero, the noise is greatly reduced without affecting any of the important information in the data [23]. The reason the threshold is not applied on the approximation is because that would alter the general structure of the signal data which wound in turn change the information encoded within it. The noise threshold T_i of each detail level is computed as [23]:

$$T = K(N)\sigma \tag{2.8}$$

$$K(N) = \sqrt{2 \ln N} \tag{2.9}$$

$$\sigma = \frac{1}{0.6745}\mathrm{MAD}\{D_i\} \tag{2.10}$$

where N is the size of the transformed data and $\mathrm{MAD}\{D_i\}$ is the median absolute deviation of the coefficients in the detail data of level i.

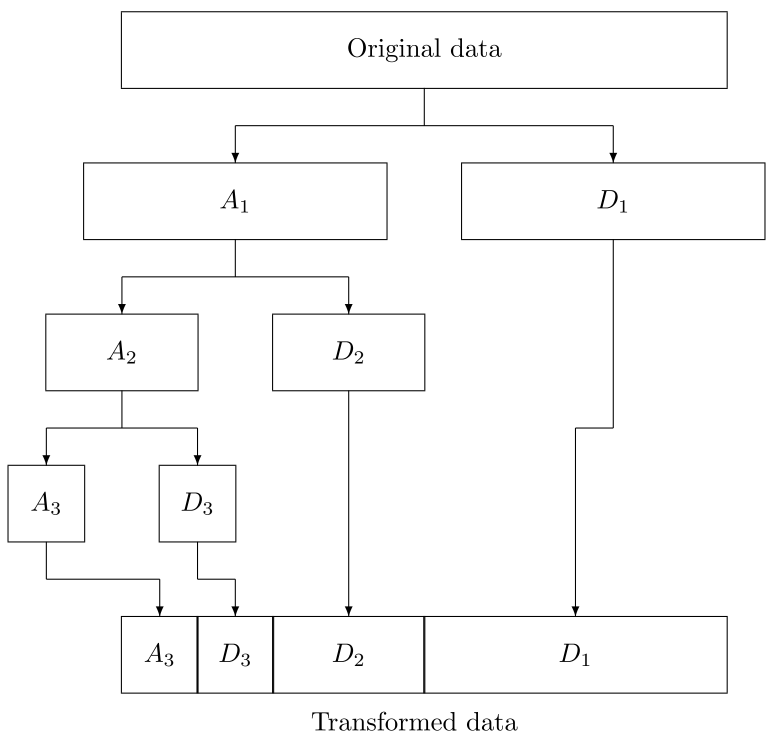

Figure 2.2: Block diagram of the data decomposition in the Wavelet transform.

Chapter 3

Methodology

This chapter introduces the equipment and software that was used to perform the radar measurements and process the measurement data. It then describes how the data is processed and how the gait parameters are extracted from the resulting data structures. The chapter concludes with a description of the tests that were conducted and how the ground truth, the reference values that are assumed to be true and to which the extracted parameters are compared to, was determined.

3.1 Equipment

The radar system that was utilized in this thesis was the USRP-2901 which is a Software Defined Radar (SDR) system made by National Instruments, shown in Figure 3.1. The functionality of the USRP-2901 system is programmable through LabVIEW, and for this thesis the system was operating on software that had already been developed. This software configured the radar system as a CW Doppler radar and enabled the user to manually define a variety of system parameters before each measurement is performed. These parameters include, but are not limited to, carrier frequency, sample frequency, number of samples, transmitter gain and receiver gain. In this thesis the sample frequency was selected as $100\,kHz$, the number of samples was set to 10^6 (one million) samples, which together with the sample frequency provided a $10s$ measurement duration. The transmitter and receiver gains were set to $25\,dB$ and $20\,dB$ respectively. The carrier frequency of the radar signal was chosen to be $2.45\,GHz$, the reason for which is given in the next paragraph.

Two antennas were used perform the measurements, one for transmitting the CW radar signal and one for receiving the return signal. This pair of antennas were of the same kind as the antenna that was developed by S. M. Moghaddam et al. [24], shown in Figure 3.2. These are dual-polarized bow tie antennas that provide a conical coverage. The selection of carrier frequency was determined based on the reflection coefficient of the antennas, which led to the choice of $2.45\,GHz$. This value is not the optimal choice in terms of reflection coefficient because the lowest coefficient occurs at $2.8\,GHz$. However the reflection coefficient at $2.45\,GHz$ is still close to the optimal value while providing the additional benefit of utilizing a frequency that falls within the Industrial, Scientific and Medical (ISM) band between 2.4 GHz and 2.5 GHz.

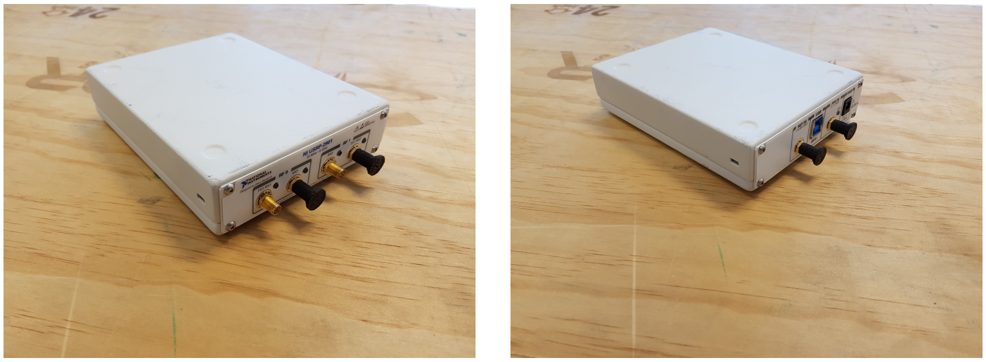

(a) Front view of the radar system (b) Back view of the radar system

Figure 3.1: The radar system used in the thesis

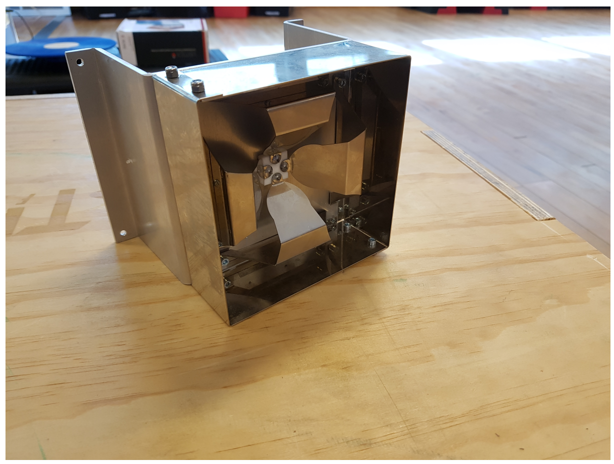

Figure 3.2: The kind of antenna used to transmit and recieve the radar singal

After a measurement has been performed the system software stores the collected samples in a file in the form of complex numbers, where the real and imaginary parts respectively correspond to the In-phase and Quadrature components of the signal. The signal processing of this data is then performed in Matlab, which is described in detail below.

3.2 Data processing

The complete data processing procedure of extracting the gait parameters from the data is shown in Figure 3.3, along with the parameters that are extracted at the end.

3.2.1 Downsampling of data

The first step in the data processing procedure is to downsample the signal from 100 kHz to 500 Hz. This is done because the original sampling frequency of 100 kHz covers a frequency range of $\pm 50\, kHz$ in accordance with the Nyquist theorem, which according to equation (2.4) correspond to a velocity

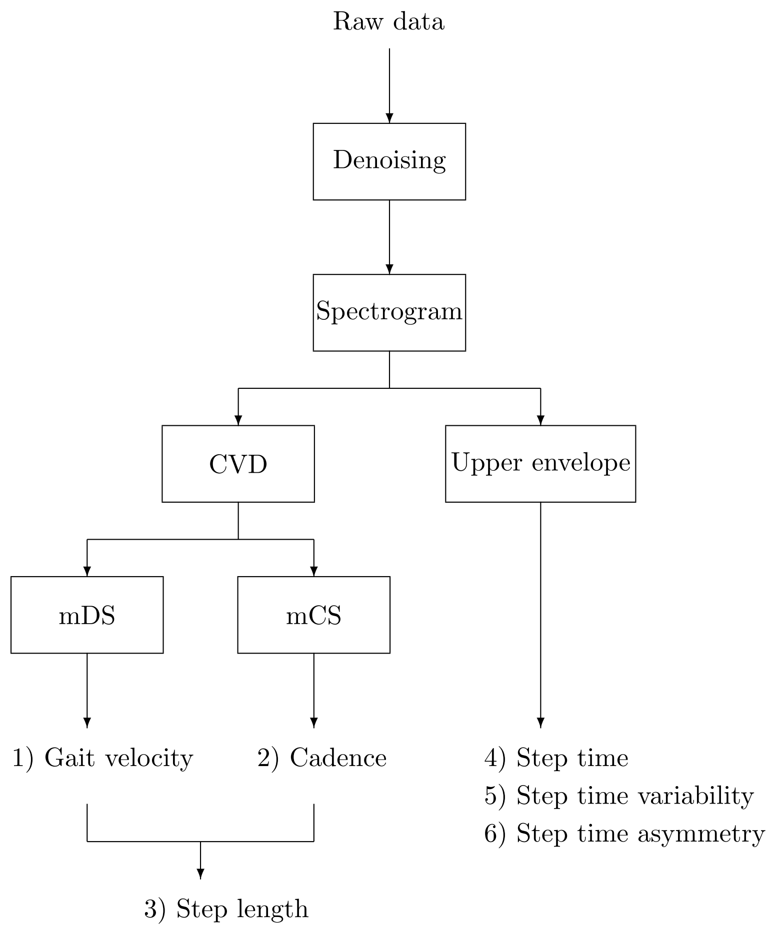

Figure 3.3: Block diagram of gait parameter extraction

range of $\pm 3061\, m/s$ due to the chosen carrier frequency. Clearly, the vast majority of this range would never be relevant since no realistic human movement would ever require such a wide range. Thus, 500 Hz was selected as a new sampling frequency after downsampling, which correspond to a velocity range of $\pm 15.3\, m/s$. This value was chosen because it greatly reduces the covered frequency range while still providing enough sample points to accurately resolve the frequency behavior of the signal when computing the Spectrogram. The reason for downsampling the signal at this stage rather than performing the measurement with a sampling frequency of 500 Hz is because the provided SDR software would coerce the sample frequency to $62.5\, kHz$ whenever it was set to a lower value. During this stage of the data processing the mean of the signal is also removed, which is done to eliminate the influence of the DC component and leave only the Doppler frequencies in the signal.

3.2.2 Data denoising

The next step in the procedure is to remove the influence of noise on the data as much as possible, which is assumed to be additive, white, and Gaussian noise (AWGN). A common method of removing such noise is by applying a moving average on the data, which is also known as Smoothing. However, a drawback of Smoothing is that it erases the finer details of the signal it is applied to, which in this context is particularly undesirable since it is within those details that the micro-Doppler signatures are encoded. A more effective method for removing AWGN while preserving the structure of the signal is to utilize the Wavelet transform. In this project, this denoising technique was applied to the FT of the data rather than the time domain signal. This method does not produce a conflict with the assumption about the noise since AWGN transforms into itself under the FT and will thus remain AWGN.

Figure 3.4 presents a comparison between four verions of the same Spectrogram in order to illustrate the effect of different denoising techniques. The Spectrogram in Figure 3.4a shows the effects of not applying any denoising techniques, the Spectrogram in Figure 3.4b shows the effects of Smoothing, the Spectrogram in figure 3.4c shows the effects of using the Wavelet transform to denoise the time domain signal, and the Spectrogram in Figure 3.4d shows the effects of using the Wavelet transform to denoise the FT of the signal. The Spectrograms are presented in decibels in order to better illustrate the effects of the different denoising techniques. The negaitve effects of smoothing can clearly be seen in 3.4b where the distinct oscillating pattern of the micro-Doppler signatures are almost completely erased. Figure 3.4c shows that some artifacts caused by high energy noise still remain after the Wavelet denoising technique has been applied to the time domain signal, appearing as vertical lines in the Spectrogram. This leaves the method of applying the Wavelet denoising technique on the FT of the signal as the clearly superior choice.

The reason that the Wavelet denoising technique produces better results when applied to the FT of the signal is hypothesized to be because the localized white noise that appear as vertical lines is significant enough, i.e the local Signal-to-Noise Ratio (SNR) is sufficiently low, so that this noise is mapped onto Wavelet coefficients that exceed the threshold and are thus not identified as noise. Evidence for this can be seen in 3.4c where the noise in between the vertical lines has definitely been reduced. However, in the Fourier domain this noise is equally prevalent in all frequencies and is thus mapped onto coefficients in the Wavelet transform that do not exceed the threshold.

3.2.3 Computation of the Spectrogram

When the data has been denoised, the next step is to compute the Spectrogram of the data as defined by equation (2.6). The applied window is a Hamming window with a length of 128 samples which correspond to $0.256s$ and the overlap between successive windows is 127 samples, which together provides a time resolution of $0.002s$. Each window is zero-padded so that the Fourier transform provide 4096 discrete frequency points, resulting in a frequency resolution of $0.12\ Hz$ which correspond to a velocity resolution of $0.0075m/s$ in accordance with equation (2.4). The Spectrogram is then smoothed using a rectangular moving average filter in order to remove some of the protrusions at the edges of the micro-Doppler signatures, with a size of 9×17 pixels that correspond approximately to $0.0675m/s$ and

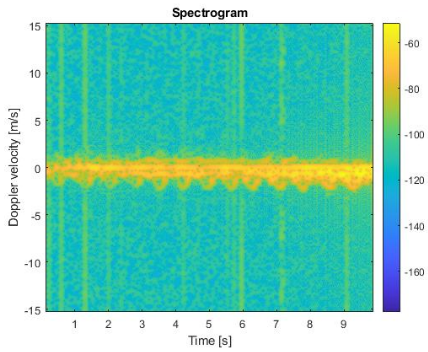

(a) No denoising

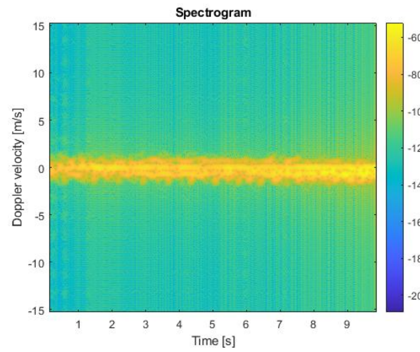

(b) Signal smoothing

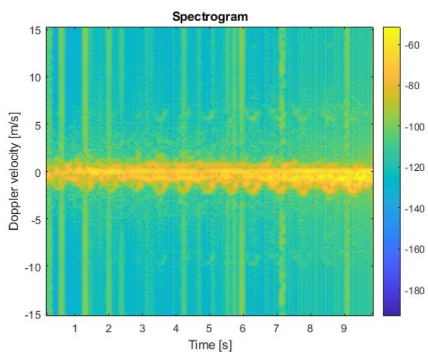

(c) Wavelet denoising in time domain

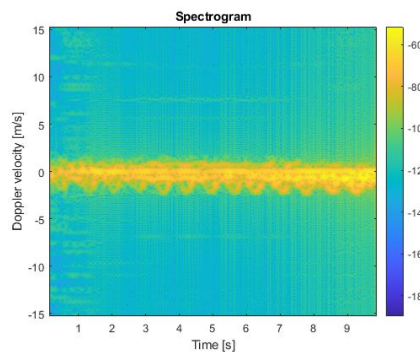

(d) Wavelet denoising in frequency domain

Figure 3.4: A comparison between the results of different denoisig methods

$0.034\,s$ respectively. Finally, an energy-based threshold is then applied to the Spectrogram in order to isolate the micro-Doppler signatures for further processing, similar to what was doe by Y. Kim and H. Ling [25]. The threshold is determined by performing a measurement without a person present in the space covered by the radar, and then a histogram is computed from the Spectrogram with its energy converted to decibels. This histogram is then compared to a histogram from a measurement where a walking person was present, and the threshold is selected as the energy where the latter histogram begins to diverge from the former. An example of a fully processed Spectrogram is shown in Figure 3.5.

3.2.4 Computation of the CVD

From the Spectrogram, the corresponding CVD is computed in the manner defined by equation (2.7). Before the Fourier transform is applied, each discrete Doppler frequency is zero-padded in order to properly resolve the Doppler repetition frequency, providing a resolution of approximately $0.0205\,Hz$. The mean of each discrete Doppler frequency is also removed before the application of the Fourier transform in order to remove the influence of the DC component. The CVD computed from the Specrtogram in Figure 3.5 is shown in Figure 3.6.

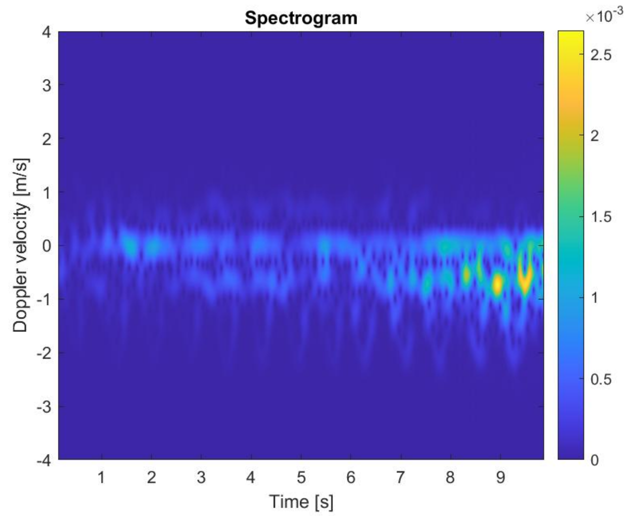

Figure 3.5: Example of a Spectrogram

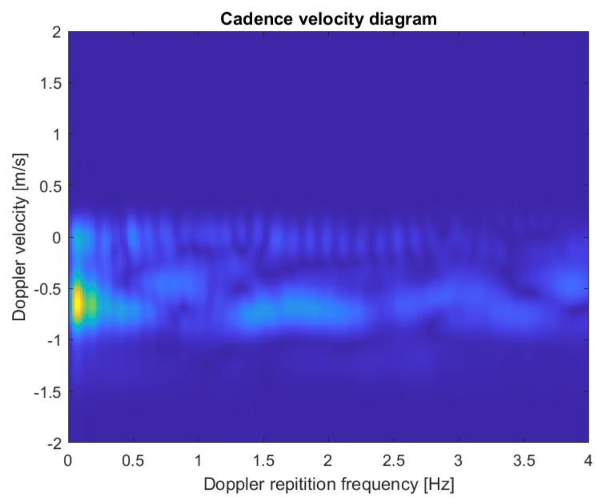

Figure 3.6: The CVD computed from the Spectrogram in Figure 3.5

3.2.5 Computation of the upper envelope

The upper envelope of the micro-Doppler signatures is equivalent to the foot envelope and thus encapsulates all micro-Doppler signatures generated by a person. The envelope is computed by first creating a binary image of the Spectrogram. This is done by first segmenting the Spectrogram along the time axis into one-second chunks, and then normalizing the energy of each individual segment. Another energy based threshold is then applied to this normalized Spectrogram in order to ensure that the micro-Doppler signatures are isolated from the background. The binary image is then created by setting every zero and non-zero element to logical zeros and ones respectively. Once the binary image is formed, every pixel cluster with up to 32000 pixels are removed in order remove any remaining noise that remained after the energy threshold, leaving a binary mask of the micro-Doppler signatures. Then for each point in time, the distances from the zero-frequency to each edge of the mask is calculated and the upper envelope is set as the absolute value of the maximum distance for each point in time. The envelope is then smoothed using a moving average with a size corresponding to 0.042 s. The upper envelope of the Spectrogram from Figure 3.5 is shown in Figure 3.7.

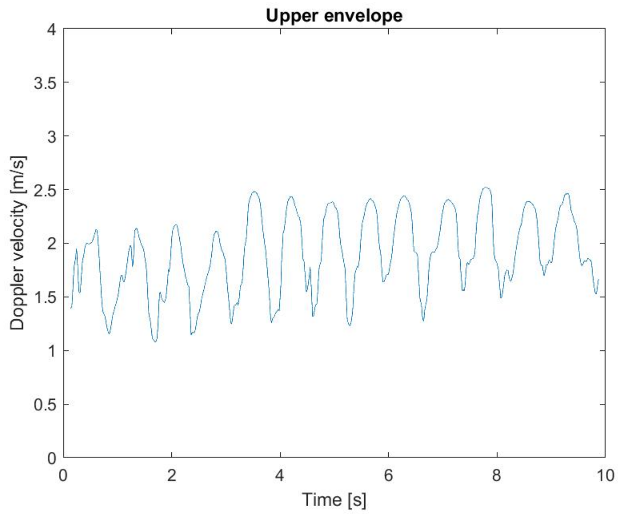

Figure 3.7: The upper envelope caomputed from the Spectrogram in Figure 3.5

3.3 Extraction of gait features

As can be seen in Figure 3.3, the system extracts a total of six gait parameters from the measurement: gait velocity, cadence, step length, step time, step time variability, and step time asymmetry.

The gait velocity refers to the average walking speed of the target and is extracted from the mean Doppler Spectrum (mDS), which is computed as the mean energy of each Doppler frequency in the CVD [16]. The most prominent peak in the mDS that is not near the zero-frequency will occur at the Doppler frequency that is caused by the gait velocity. This peak is then identified and the corresponding frequency is converted into velocity, which in turn is set as the gait velocity. The mDS that is computed from the CVD in Figure 3.6 is shown in Figure 3.8 where the peak corresponding to the velocity is clearly visible.

The cadence refers to the average number of steps per second taken by the target and is extracted from the mean Cadence Spectrum (mCS), which is computed as the average energy of each Doppler repetition frequency in the CVD [16]. The mCS is then smoothed using a filter with a size corresponding to 0.18 Hz. The peaks in the mCS correspond to the harmonic components of the gait, where the highest peak in the mCS corresponds to the oscillating movement of the torso while the second highest peak in the mCS, i.e. the first harmonic, tend to correspond to the oscillating motion of the legs in the case of unassisted gait, as described in Section 2.3. Thus the next step in extracting the cadence is to identify the second highest peak in the mCS and then set the corresponding Doppler repetition

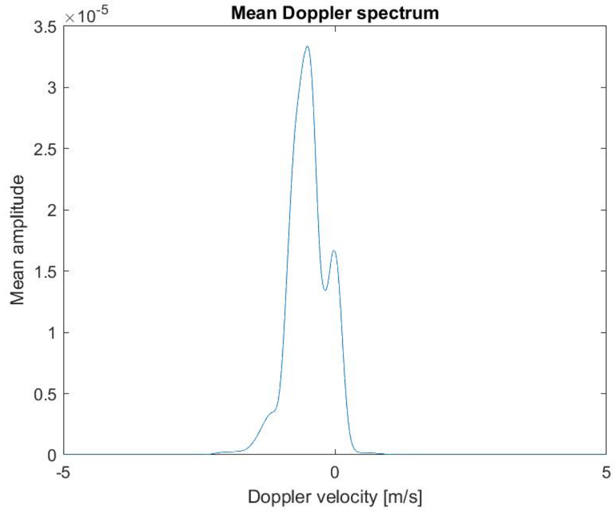

Figure 3.8: The mDS computed from the CVD in Figure 3.6

frequency as the cadence. The mCS computed from the CVD in Figure 3.6 is shown in Figure 3.9 where the second highest peak is seen around 1.5 Hz. The extracted values of the gait velocity and the cadence can be used to estimate the step length, which is the distance covered with a single step,by calculating the ratio between the gait velocity and the cadence [20].

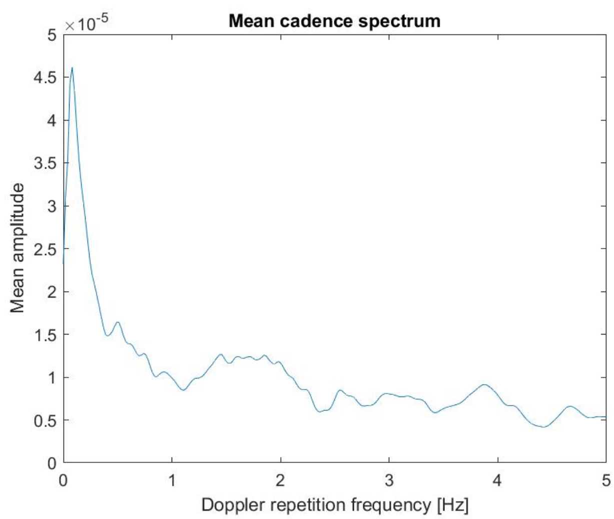

Figure 3.9: The mCS computed from the CVD in Figure 3.6

The remaining parameters to be extracted are the step time which refers to the average time it takes to perform a single step, the step time variability which describes how much variation there is in the step times, and step time asymmetry which measures the average difference between the step time of the right and left leg. The first step in extracting these parameters is to identify the steps taken by the subject during the measurement, which correspond to the most prominent peaks in the envelope. An example of an envelope where the step identification has been applied is shown in Figure 3.10 where the red markers show the peaks that the system has identified as steps. When the steps have been identified the parameters are estimated as follows: The step time is calculated as the mean of the time differences between successive steps, and the step time variability is calculated as the standard deviation off the same time differences. Finally, the step time asymmetry is calculated by taking successive pairs of step times and computing the absolute difference of each pair as described by the following equation:

$$t_{asym} = \frac{1}{n}\sum_{k=1}^{n} |t_{step,2k-1} - t_{step,2k}| \tag{3.1}$$

where $t_{step,i}$ refers to the ith step time and n is the number of pair of step times. This corresponds to computing the absolute difference between each pair of right and left step times, and then the mean value of these differences are calculated.

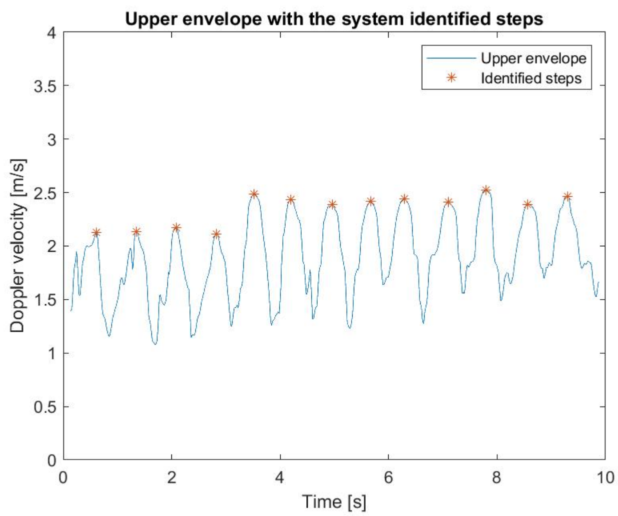

Figure 3.10: The upper envelope from Figure 3.7 where each step identified by the system is marked

3.4 Conducted tests

The developed radar system was tested in two phases in order to determine its reliability as a potential in-home gait monitoring system. Across these phases the measurements were collected in three different measurement scenarios. During the first phase the system was deployed in an ideal environment, which also served as the first measurement scenario, in a similar manner as previous studies where the space covered by the radar was empty of any objects that could potentially interfere with the measurement in some way. The transmitting and receiving antennas were placed next to each other at a height of 0.51 m above the ground. Directly in front of the antennas a line was measured out that extended radially away, where each half-meter interval was marked with tape. During the tests the subject was asked to walk along this line either towards or away from the antennas, while taking care to place the foot at the markers with each step. The measurement setup utilized during this phase is shown in figure 3.11. In each conducted test the subject crossed the distance between the 1 m marker and the 8 m, or vice versa, while adopting one of four predefined gait patterns. These patterns were a normal walk at paces that the subject considered to be slow, medium, and fast paces, along with simulated limping which was performed by keeping one knee stiff during the movement.

Figure 3.11: The test setup in the ideal environment

In the second phase the developed system was deployed in a space meant to simulate a home environment, i.e. there are objects present within the space covered by the radar antennas. In the tests that were conducted during this phase, the subject adopted the same gait patterns as in the previous phase while walking either towards or away from the radar antennas. During this phase the remaining two measurement scenarios were investigated, with the first being when the radar has a clear line of sight of the target and the second being when there is clutter that obscures the line of sight. In the latter case the distance that the subject covers during the measurement is reduced due to the objects blocking the path. The measurement setup for the two scenarios within the simulated home environment is shown in figure 3.12.

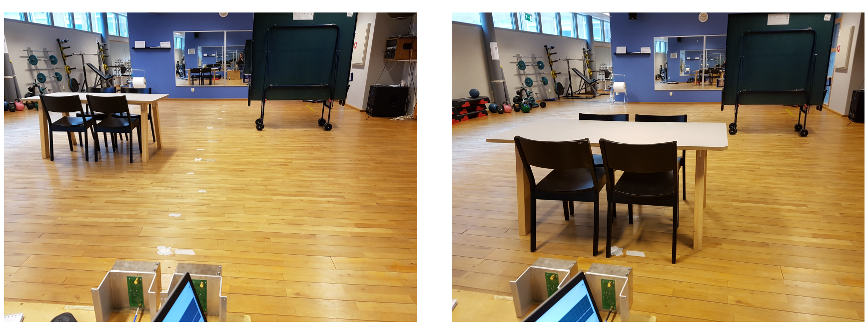

(a) Simulate home environment with clear line of sight

(b) Simulate home environment with obscured line of sight

Figure 3.12: The test setup in each case in the simulated home environment

During both phases the measurements were video recorded using a mobile phone with the consent of the subject. The videos were recorded at 30 frames per second and thus provide a time resolution of 0.033 s. From these recordings some gait parameters were estimated, the same gait parameters as those extracted by the system, and were held as the ground truth to compare against the parameters extracted by the system. The ground truth is estimated from the time instances of each heel-strike, the moment when the heel makes contact with the ground, which was determined manually by eye. The time instances of the heel-strikes are also determined manually by stepping through the videos frame by frame, keeping count of the number of frames and noting down the frame number when the heel-strike occurs, along with the minute and second.

Chapter 4

Results

This chapter presents the results of the preformed tests as two comparisons, one between the utilized measurement scenarios and the other between the adopted gait patterns. These comparisons are made based on parameter deviation, the differences between the extracted parameters values from each case and their corresponding reference values. A description of how the statistical representation of these differences are computed and how to interpret them are included at the beginning of the chapter.

4.1 Statistical representation of the results

The extracted parameters are used to determine the system performance by comparing them in two different contexts. The first comparison is between the three different measurement scenarios described in Section 3.4 in order to determine the impact on reliability in the simulated home environment relative to the ideal environment. The second comparison is between the four different gait patterns that were adopted during the measurements in order to determine how well the system performs for each pattern. These comparisons are made on the basis of the parameter deviation, which is referring to the difference between the value of the extracted parameters and the corresponding value in the ground truth. The desired deviation for all parameters is zero since that means that the parameter value extracted from the measurement data matches the ground truth exactly.

The deviations of each parameter is presented in the form of boxplots, which represent the data in the following way [26]: the line inside the rectangle (box) marks the median of the data set. The edges of the box, called the quartiles, approximately mark the 25 percentile and 75 percentile of the data. The range covered by the box is called the interquartile range (IQR), containing approximately 50 % of the data. The data points that fall outside the box but is no further away from the edges than 1.5(IQR) in the respective directions are covered by the line segments, called whiskers. Any data that are not covered by the box or whiskers are considered outliers and are marked with a small circle. Figure 4.1 shows a simple illustration of an example boxplot. This method of presenting the results was chosen because it is resistant to outlier data since it is based on the median, unlike the mean which is very sensitive to outliers, and it also enables the identification of such data. In each figure that contain boxplots, the corresponding parameters are ordered in the following way: 1) Gait velocity [m/s], 2) Cadence [Hz], 3) Step length [m], 4) Step time [s], 5) Step time variability [s], 6) Step time asymmetry [s].

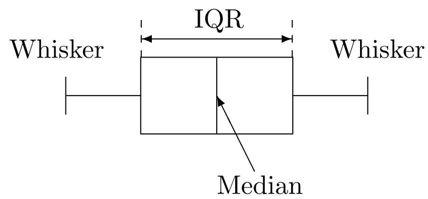

Figure 4.1: Illustration of a boxplot

4.2 Comparison between measurement scenarios

The comparison of the measurement results based on the measurement scenarios is presented in Figure 4.2, where Figure 4.2a shows the results from the measurements performed in an ideal environment, and where Figure 4.2b and Figure 4.2c show the results from the simulated home environment with a clear and obstructed line of sight respectively. These figures were compiled using 24, 24, and 16 measurements for each respective measurement scenario, and each figure includes measurements of every utilized gait pattern since this comparison is made between the different scenarios only, regardless of which gait pattern was adopted in the measurements.

The lengths of the intervals between the ends of the whiskers and the lengths of the intervals between the quartiles of the boxplots in Figure 4.2 are presented in Tables 4.1 and 4.2 respectively for each parameter. The scenarios in the tables refer to the measurement scenarios and are ordered in the following way: Scenario 1 - the ideal environment, Scenario 2 - the simulated home environment with a clear line of sight, Scenario 3 - the simulated home environment with an obstructed line of sight. The gait parameters in these tables are ordered in the same way as they are in the boxplots. When comparing these interval lengths with each other it can be seen that the values under each parameter are fairly similar to each other. The exception to this are the values under the Step time parameter in Scenario 3, where in both tables they is approximately one magnitude larger than the other values. When regarding the interval lengths from the two scenarios that are performed in the simulated home environment, one can see that in general the interval lengths in Scenario 2 are lower than the corresponding values in Scenario 3, which holds for both tables. Comparing the values from the two previous scenarios with the corresponding in Scenario 1 shows that the values in Table 4.1, i.e. the interval length between the whiskers, are in general smaller in Scenario 1. However, the interval lengths between the quartiles from the same measurement scenario in Table 4.2 does not show a general trend as to which environment results in smaller interval lengths. In this table the parameters derived from the CVD have smaller interval lengths in Scenario 2 and Scenario 3, while the parameters derived from the upper envelope have smaller interval lengths in Scenario 1.

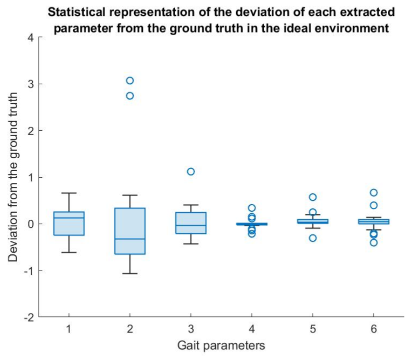

(a) Deviation from ground truth in ideal environment

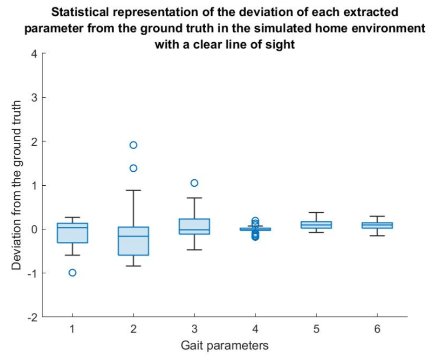

(b) Deviation from ground truth in a simulated home environment with clear line of sight

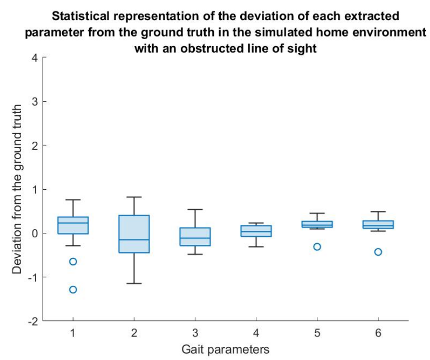

(c) Deviation from ground truth in a simulated home environment with obstructed line of sight

Figure 4.2: Parameter deviations from the ground truth in each measurement scenario. The parameters are ordered as follows: 1) Velocity, 2) Cadence, 3) Step length, 4) Step time, 5) Step time variabiity, 6) Step time asymmetry

Table 4.1: The interval lengths between the whiskers of each parameter from the boxplots of Figure 4.2

	Velocity	Cadence	Step length	Step time	Step time variability	Step time asymmetry
Scenario 1	1,2712	1,6822	0,8286	0,05142	0,29557	0,2743
Scenario 2	0,8678	1,7151	1,1883	0,09939	0,4553	0,4440
Scenario 3	1,0399	1,9597	1,0137	0,5469	0,35924	0,45113

4.3 Comparison between gait patterns

The comparison of the measurement results between the different gait patterns is presented in Figure 4.3, where Figure 4.3a show the results from the measurements of a slow pace, Figure 4.3b shows the

Table 4.2: The interval lengths of the IQR of each parameter from the boxplots of Figure 4.2

	Velocity	Cadence	Step length	Step time	Step time variability	Step time asymmetry
Scenario 1	0.4928	0.9845	0.4501	0,02798	0,07759	0,08886
Scenario 2	0,4362	0,64238	0,3419	0,04137	0,15225	0,12881
Scenario 3	0,38913	0,8486	0,3962	0,24612	0,1313	0,1796

results from the measurements of a medium pace, Figure 4.3c shows the results from the measurements of a fast pace, and Figure 4.3d shows the results from the measurements of imitated limping. These figures were compiled using 17, 16, 14, and 17 measurements respectively for each gait pattern, and each figure includes measurement from every measurement scenario since this comparison is made between the different adopted gait patterns, regardless of which scenario the measurements were performed in.

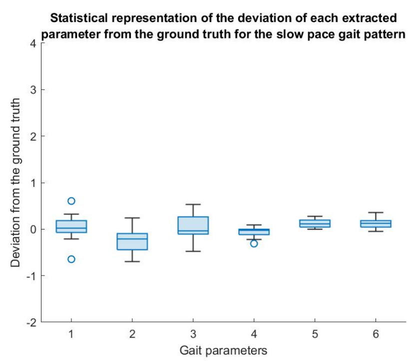

(a) Deviation from ground truth for slow pace

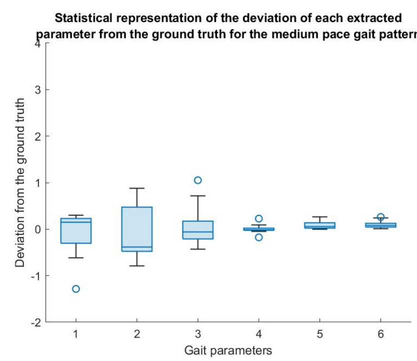

(b) Deviation from ground truth for medium pace

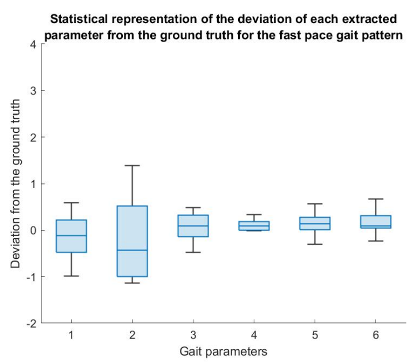

(c) Deviation from ground truth for fast pace

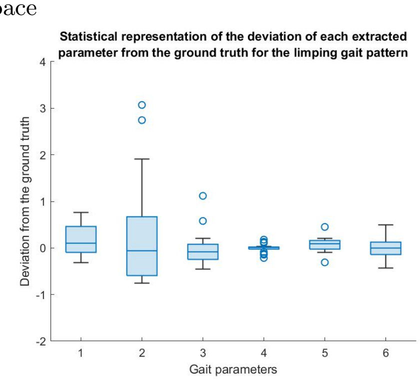

(d) Deviation from ground truth for limp pace

Figure 4.3: Parameter deviations from the ground truth for each gait pattern. The parameters are ordered as follows: 1) Velocity, 2) Cadence, 3) Step length, 4) Step time, 5) Step time variabiity, 6) Step time asymmetry

The lengths of the intervals between the ends of the whiskers and the lengths of the intervals between the quartiles of the boxplots in Figure 4.3 are presented in Tables 4.3 and 4.4 respectively for each parameter. The parameters are again ordered in the same way as in the boxplots. When comparing the interval lengths of the gait patterns that are the three different paces, it can be seen that in general the slow pace has the smallest interval length under the first three parameters in both tables. The medium pace show an increase in the interval lengths under the same parameters in both tables, but also shows a slight decrease in the interval values under the last three parameters compared to the results from the slow pace. The fast pace shows the largest interval lengths in both tables for all parameters among the three compared gait patterns with the exception of the value under Step length in Table 4.3, which is the smallest of those interval lengths. When comparing the last gait pattern, Limping, to the other gait patterns, one can see that the interval lengths are in general similar to either the highest or second highest values from the other gait patterns. The exception to this are the interval lengths under the Step length and Step time parameters where the this gait pattern holds the lowest values in both tables.

Table 4.3: The interval lengths between the whiskers of each parameter from the boxplots of Figure 4.3

	Velocity	Cadence	Step length	Step time	Step time variability	Step time asymmetry
Slow pace	0,5368	0,9336	1,0137	0,31947	0,275181	0,41053
Medium pace	0,9054	1,6688	1,1411	0,13437	0,263452	0,22484
Fast pace	1,5793	2,528	0,9548	0,35397	0,8771	0,9032
Limping	1,0713	2,6669	0,6601	0,05547	0,30357	0,9209

Table 4.4: The interval lengths of the IQR of each parameter from the boxplots of Figure 4.3

	Velocity	Cadence	Step length	Step time	Step time variability	Step time asymmetry
Slow pace	0,25299	0,34721	0,3735	0,112352	0,14681	0,14608
Medium pace	0,5299	0,95	0,3765	0,0543	0,12544	0,08258
Fast pace	0,6972	1,5091	0,4694	0,183619	0,25558	0,25978
Limping	0,55476	1,2592	0,31469	0,04163	0,17945	0,2598

Chapter 5

Discussion

In this chapter, the comparisons made in Chapter 4 are used to to discuss the impact that the different measurement scenarios and gait patterns have on the system performance in terms of reliability. Included in the discussion is an explanation of why some measurements were excluded from the results and how the method for determining the ground truth may have caused some inherent deviation in the results. The chapter then concludes with some suggestions for future work.

5.1 Experimental results

5.1.1 Comparison between the measurement scenarios

From the comparison of the results between the different measurement scenarios in Section 4.2, it is reasonable to say that the reliability of the system within each of the two scenarios in the simulated home environment are very similar to each other. In general the third measurement scenario, the one with an obstructed line of sight, results in somewhat higher interval lengths in both Table 4.1 and Table 4.2, indicating a decrease in reliability which is likely because the obstruction causes additional attenuation in the radar signal. The reason that this decrease in reliability is not particularly significant is because the carrier frequency of the radar signal is sufficiently low to penetrate the obstruction. An exception to the similarity between the two measurement scenarios are, as mentioned in Section 4.2, the values under the parameter Step time for Scenario 3 in both tables where it is quite larger than the vales in the other two measurement scenarios. However, since this disparity does not appear under any other parameter for Scenario 3 in either table, and since the other interval lengths of the parameters related to the step times in Scenario 3 are similar to the corresponding values in Scenario 2 in both tables, it seems reasonable to assume that this an anomaly rather than an indication of the system performance in the third measurement scenario. Comparing these results from the simulated home environment with those from the ideal environment shows that the interval lengths between the whiskers are in general smaller in the ideal environment while neither environment shows generally smaller values of the IQR lengths. This indicates that the system is slightly more reliable in the ideal environment since the total spread of the data, excluding outliers, is in general smaller in this environment. Thus the presence of clutter does seem to have a negative impact on the reliability of the system relative to the ideal environment, however the difference in reliability between the environments is very small and is not a significant factor in the overall performance of the system. This implies that the system would be able to operate in a home environment assuming that it is sufficiently reliable in an ideal environment.

5.1.2 Comparison between the gait patterns

From the comparison between the different gait patterns in Section 4.3, it is reasonable to say that the reliability of the system seems to decrease as the pace, and thus the velocity of the feet, increases. The gait parameters that are more affected by this are those derived from the CVD, which suggests that the issue lies with the energy of the micro-Doppler signatures generated by the legs. When the legs are moving at a faster velocity then the reflected energy is spread out over a larger range of discrete Doppler frequencies in the Spectrogram compared to a slower leg velocity, which means that there is less energy contained within a single discrete Doppler frequency than there is for a slower leg velocity. This effectively means that the micro-Doppler signatures generated by a faster pace has a lower SNR than those generated by a slower pace. If the SNR is not high enough to distinguish the micro-Doppler signatures from the background in the Spectrogram, then the periodic pattern of the gait will not be resolved in the CVD and thus a prominent peak will not arise in the the mCS or the mDS, making it difficult or even impossible to extract the corresponding parameters. The lower SNR of a faster pace would also affect the computation of the upper envelope because of the energy threshold used to isolate the micro-Doppler signatures in the Spectrogram by removing some of the signatures along with the background. Figure 5.1 presents a comparison between two mCS plots and two mDS plots in order to illustrate the effect of low SNR on the extraction of the velocity and the cadence. The plots in Figure 5.1a and Figure 5.1b show the mCS and the mDS respectively from a measurement where the slow pace was adopted, and as can be seen the peaks that correspond to the cadence and velocity are easily identifiable in each respective figure, as described in Section 3.3. The plots in Figure 5.1c and Figure 5.1d show the mCS and mDS respectively from a measurement where the fast pace was adopted, and as can be seen there no discernible peaks that would correspond to the cadence and velocity in each respective figure. This indicates that the reliability of the system is far more dependent on the SNR of the micro-Doppler signatures, especially those generated by the legs, than it is on any clutter present within the space covered by the radar.

When comparing the results of the limping pattern to the other gait patterns it is clear that the reliability of the system is quite poor, on par with the fast pace pattern. This poor reliability mainly affects the parameters derived from the CVD, especially the cadence. While this result might in part be caused by poor quality in the data, another factor may in fact be that the developed system is unable to properly process this gait pattern because the system is too simplistic in the sense that the assumptions that the parameters extraction procedure is based on do not hold for more complex gait patterns like limping. Limping is characterized by a slow step that is shortly followed by a quick step, which generate micro-Doppler signatures that appear in the Spectrogram as peaks of alternating height. It is this characteristic alternating pattern between high and low peaks in the Spectrogram

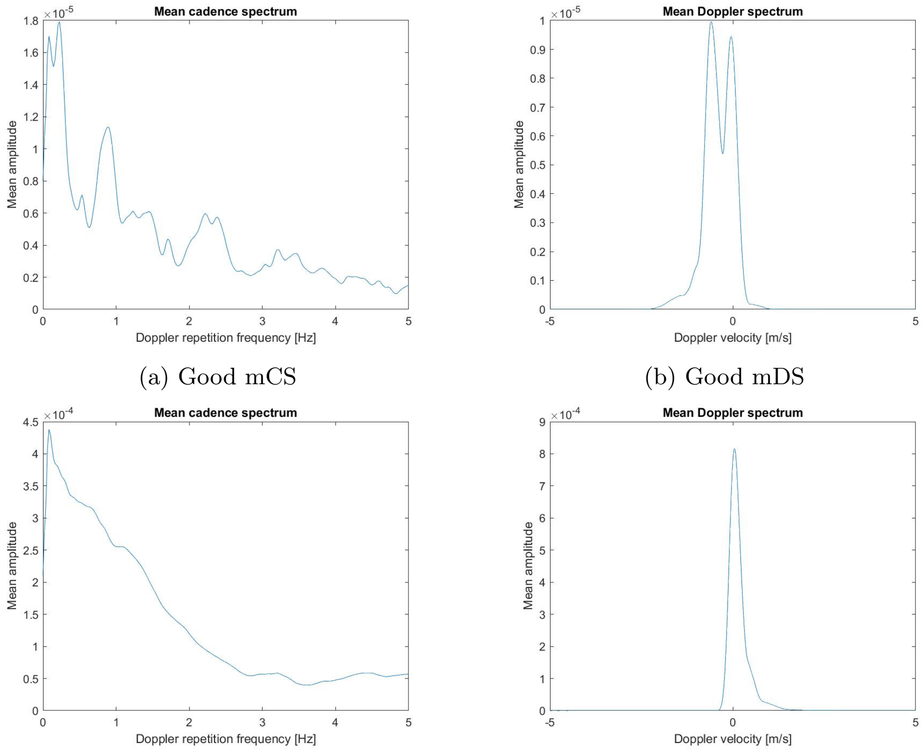

(a) Good mCS (b) Good mDS

(c) Bad mCS (d) Bad mDS

Figure 5.1: A comparison between a pair of mCS and mDS plots where value to be extracted is clear, and a pair where it is ambiguous

that causes issues in the extraction of the cadence from the CVD. This is because there will be some Doppler frequencies where only the micro-Doppler signature generated by the faster step are present, so when the Fourier transform is applied to compute the CVD only the repetition of the faster step will be detected in these frequencies. This results in two different prominent Doppler repetition frequencies in the mCS: one that correspond to the cadence and one that correspond to the repetition frequency of the faster step. Contrast this with the usual single peak that is generated by a normal walking pattern which is what the system is assuming will happen, as explained in Section 3.3. Thus if the peak in the mCS that is caused by the faster leg alone is higher than the peak corresponding to the cadence, then the system will select that Doppler repetition frequency as the cadence since it is looking for the second highest peak. This is illustrated in Figure 5.2 where the upper envelope from a measurement where the limping pattern was adopted is shown, along with the corresponding mCS where two different peaks can be seen, apart from the peak generated by the motion of the torso, appearing around $0.5\,Hz$ and $1\,Hz$.

5.1.3 Sources of error

Some of the parameter deviations will also be caused by the ground truth itself due to how it was calculated from the video recordings. Since it depends on the manual counting of frames and the

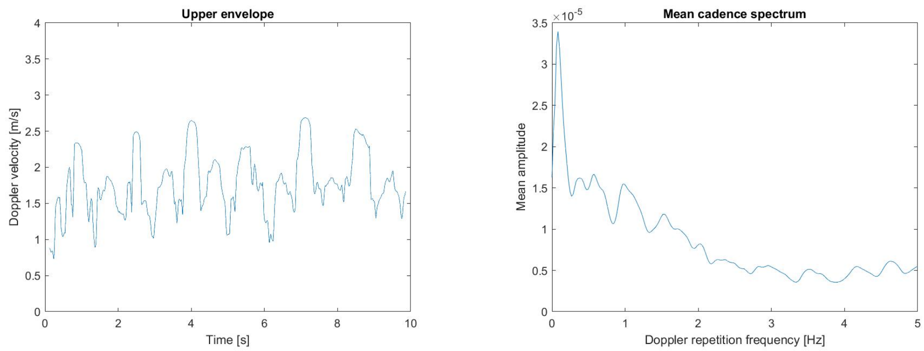

(a) The envelope of limping (b) The mCS of limping

Figure 5.2: An example of a measurement of limping, displaying the inherent pattern of such a gait and the periodicities it generates

somewhat subjective judgement of when exactly a heel-strike has occurred in the video, the calculated ground truth may be off by a frame or two compared to reality, which corresponds to a potential offset of $\pm 0.033s$ to $\pm 0.067s$ for each heel-strike. This offset would not have a significant impact on the gait velocity or the cadence values since these values only depend on the time interval between the first and last heel-strikes. However, this offset would have a more significant impact on the parameters derived from the upper envelope, especially the step time variability and the step time asymmetry since these parameters operate on the same scale as the time resolution of the video recordings. However, since all results share the exact same same source of error it may not be that significant because the system was evaluated based on the relative reliability between different cases rather than the absolute reliability or the accuracy compared to the ground truth.

It must be mentioned that the boxplots in Figures 4.2 and 4.3 were not compiled using all available measurements, some were purposefully excluded in order to gain a more accurate understanding of the systems capabilities. Every excluded measurement is of the same nature, which is that the I/Q components of the measurement data appear very similar to pure, phase-shifted sinusoidal waves. An example of this is shown in Figure 5.3, with the impact this phenomenon has on the Spectrogram, envelope, mCS, and mDS, shown in Figure 5.4. As can be seen, there are no meaningful values that can be extracted from these measurements since barely any micro-Doppler signatures appear to be present, which is why they have been excluded from the comparisons above. The origin of this phenomenon remains completely unknown and thus no strategies to avoid it was discovered. The total number of measurements of this kind that was excluded was 23, which means that approximately 26% of the performed measurements were unusable. This exclusion of measurements has reduced the sample sizes of the measurement subsets, which means that the comparisons of the results presented in Chapter 4 may not fully reflect the true relationship between the different measurement scenarios or gait patterns. One potential example of this could be the values under the step time parameter in Scenario 3 in both Table 4.1 and Table 4.2, which is significantly larger than in the other measurement scenarios. Another such example could be the minor decrease in the values under the last three parameters for the medium pace compared to the slow pace in both Table 4.3 and Table 4.4.

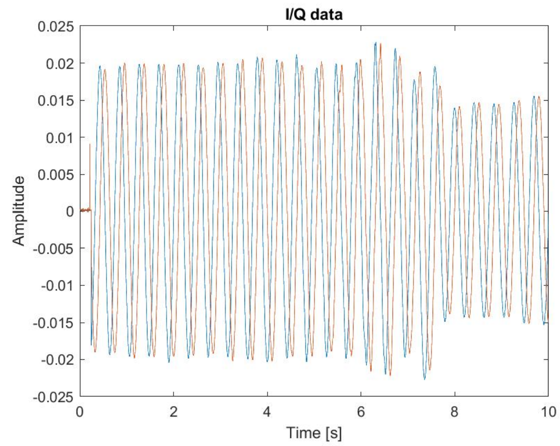

Figure 5.3: Example of the I/Q components of the measurement data for the strange phenomenon

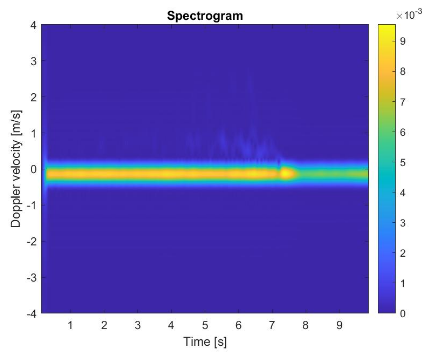

(a) The resulting Spectrogram from the data shown in Figure 5.3

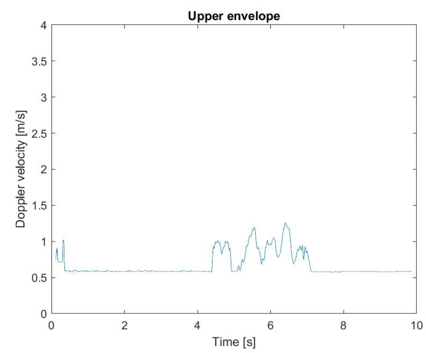

(b) The resulting envelope from the data shown in Figure 5.3

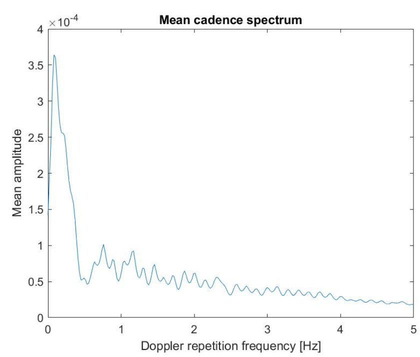

(c) The resulting mCS from the data shown in Figure 5.3

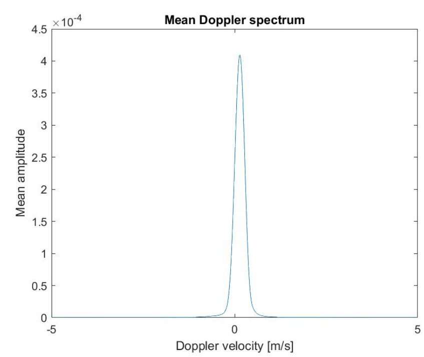

(d) The resulting mDS from the data shown in Figure 5.3

Figure 5.4: The effects of the strange phenomenon on the derived data structures used to extract the gait parameters

5.2 Future work

The most important task for future work is to investigate strategies to improve the quality of the measurement data, both in terms of increasing the SNR of the micro-Doppler signatures and eliminating the strange phenomenon where the measurement data appears as a pure sinusoid without any detectable micro-Doppler signatures. The former could potentially be done by focusing the radar coverage more towards the legs in order to better capture and resolve the micro-Doppler signatures. The latter could be done through redundancy by utilizing several antennas and radar units which would allow the system to compensate for any issues that could arise from a single antenna. It could also be done through machine learning where a network is trained to recognise and immediately discard the measurement.

Machine learning could also be used to improve upon the system by optimizing the data processing procedure and expand the number of parameters that are extracted from the measurement data. Some examples of such improvements would be to alter the energy threshold that is used to isolate the micro-Doppler signatures so that it adapts to the current measurement rather than being the static constant that it currently is. Another improvement would be to allow the system to also track the movements of the knees and arms which are very difficult to identify by eye within the Spectrogram. One final example would be to implement a procedure where a curve is fitted to the upper envelope from which additional temporal parameters can be extracted by identifying known points on the fitted curve. Another benefit of using machine learning is that the system can then be trained using simulation data of different gait patterns which alleviates the need to perform real measurements at the needed quantity to train a classifier.

In order for the developed system to be truly viable as an in-home gait monitoring system there are other system functionalities beyond data processing that must also be implemented. For example, this will include extending the system so that it is able to coordinate between several radar units in order to cover the entire room. This could potentially require some method of tracking the subject as they move throughout the home such as using motion trackers. Additionally, the coordination between units would likely necessitate expanding the measurement dimension from the current single dimension (1D) into two dimensions (2D), or in other words using at least two antennas whose views of the target are orthogonal to each other. This is because the system depends the capture of several gait cycles in order to properly resolve the gait pattern which requires the subject to cover a distance of a few meters, and such a distance may not always align with the walls within the home in such a manner where only one antenna is necessary. The extension of the measurement dimension into 2D also introduces the possibility of implementing a fall detection functionality since a fall should cause a sudden spike in the Spectrogram.

As a final suggestion for future work, an interesting avenue to explore would be the investigation the possibility of using the Wavelet transform in order to represent the time-frequency behavior of the micro-Doppler signatures, rather than using the Fourier transform. The Wavelet transform might be a more natural representation of the micro-Doppler signatures since the movement of different limbs, and thus their Doppler shifts, are more prominent on different time scales and are thus better represented by the adaptive time-frequency resolution of this transform. This investigation would involve determining the type of Wavelet that should be used, how many levels the data should be decomposed into, and how to extract the gait parameters from the transformed data.

Chapter 6

Conclusion

The aim of the thesis was to investigate the efficacy and reliability of a radar-based gait monitoring system within a home environment. A gait measurement system based on continuous wave radar was developed that was capable of extracting six gait parameters from the measurement data. This system was tested in three different scenarios: an ideal environment where no clutter was present, a simulated home environment with a clear line of sight, and a simulated home environment with an obstructed line of sight. This was done in order to determine the impact that clutter would have in the system. During each measurement one of four gait patterns was adopted: slow pace, medium pace, fast pace and limping. The system was evaluated based on the difference between the extracted values and reference values derived from video recordings.

Comparing the measurement results between the different scenarios showed that the difference in system reliability between the two measurement scenarios in the simulated home environment is negligible, while the difference in system reliability between the ideal environment and the home environments is very minor. This indicates that this type of radar would be able to operate in a home environment with only a minor decrease in reliability even if the line of sight is obscured since the radar signal is able to penetrate the clutter. Comparing the measurement results between the different gait patterns showed that the system reliability decreases with increasing leg velocity because the faster velocity effectively decreases the SNR of the micro-Doppler signatures. The system also performs poorly regarding the limping pattern because the characteristic movement of this gait pattern can confuse the system, causing it to identify incorrect values for some parameters. This indicates that strategies to better capture the micro-Doppler signatures of faster paces must be implemented and the system must be extended such that it can better process more complex gait patterns, before the system can be considered viable as an in-home gait monitoring system.

The derivation of the reference values from video recordings which depended in part on subjective judgement, may have introduced additional difference between the extracted and reference values along with the rough time resolution of the video recordings. Additionally some measurements were discarded because the presence of micro-Doppler signature were either very faint or nonexistent, which reduced the sample size.

Bibliography

[1] A. M. Z. Ann-Kathrin Seifert, Moeness G. Amin, "New analysis of radar micro-doppler gait signatures for rehabilitation and assisted living," *2017 IEEE International Conference on Acoustics, Speech and Signal Processing (ICASSP)*, 2017.

[2] M. Mercuri *et al.*, "Vital-sign monitoring and spatial tracking of multiple people using a contactless radar-based sensor," *Nature Electronics*, vol. 2, no. 6, p. 252–262, 2019.

[3] G. H. Jyothsna Kondragunta, Christian Wiede, "Gait analysis for early parkinson's disease detection based on deep learning," *Current Directions in Biomedical Engineering*, vol. 5, no. 1, pp. 9–12, 2019.

[4] Parkinson's Foundation, "Statistics," accessed: 2022-05-31. [Online]. Available: https://www.parkinson.org/Understanding-Parkinsons/Statistics

[5] S. Bridenbaugh and R. Kressig, "Laboratory review: The role of gait analysis in seniors' mobility and fall prevention," *Gerontology*, vol. 57, no. 3, p. 256–264, 2011.

[6] Centers for Disease Control and Prevention, "Facts about falls," accessed: 2022-05-31. [Online]. Available: https://www.cdc.gov/falls/facts.html

[7] F. Wang *et al.*, "Quantitative gait measurement with pulse-doppler radar for passive in-home gait assessment," *IEEE TRANSACTIONS ON BIOMEDICAL ENGINEERING*, vol. 61, no. 9, pp. 2434–43, 2014.

[8] K. Saho *et al.*, "Using micro-doppler radar to measure gait features associated with cognitive functions in elderly adults," *IEEE Access*, vol. 7, pp. 24 122–24 131, 2019.

[9] R. Parihar, J. R. Mahoney, and J. Verghese, "Relationship of gait and cognition in the elderly," *Current Translational Geriatrics and Experimental Gerontology Reports*, vol. 2, no. 3, pp. 167–173, 2013.

[10] R. Morris *et al.*, "Gait and cognition: Mapping the global and discrete relationships in ageing and neurodegenerative disease," *Neuroscience & Biobehavioral Reviews*, vol. 64, pp. 326–345, 2016.

[11] L. R. Sue Lord, Brook Galna, "Moving forward on gait measurement: Toward a more refined approach," *Movement Disorders*, vol. 28, no. 11, pp. 1534–1543, 2013.

[12] A.-K. Seifert, M. Grimmer, and A. M. Zoubir, "Doppler radar for the extraction of biomechanical parameters in gait analysis," *IEEE Journal of Biomedical and Health Informatics*, vol. 25, no. 2, pp. 547–558, 2021.

[13] B. Godana, A. Barroso, and G. Leus, "Estimating human movement parameters using a software radio-based radar," *International Journal on Advances in Systems and Measurements*, vol. 4, no. 1-2, pp. 20–31, 2011.

[14] A. M. de-la Herran, B. Garcia-Zapirain, and A. Mendez-Zorrilla, "Gait analysis methods: An overview of wearable and non-wearable systems, highlighting clinical applications," *Sensors*, vol. 14, no. 2, pp. 3362–3394, 2014.

[15] J. L. Kernec *et al.*, "Radar for assisted living in the context of internet of things for health and beyond," *2018 IFIP/IEEE International Conference on Very Large Scale Integration (VLSI-SoC)*, 2018.

[16] A.-K. Seifert, M. G. Amin, and A. M. Zoubir, "Toward unobtrusive in-home gait analysis based on radar micro-doppler signatures," *IEEE TRANSACTIONS ON BIOMEDICAL ENGINEERING*, vol. 66, no. 9, pp. 2629–2640, 2019.

[17] A.-K. Seifert, A. M. Zoubir, and M. G. Amin, "Detection of gait asymmetry using indoor doppler radar," *2019 IEEE Radar Conference (RadarConf)*, 2019.

[18] M. Z. Ram M. Narayanan, "Radar micro-doppler signatures of various human activities," *IET Radar, Sonar & Navigation*, vol. 9, no. 9, pp. 1205–1215, 2015.

[19] J. Zhang, "Basic gait analysis based on continuous wave radar," *Gait & Posture*, vol. 36, no. 4, pp. 667–671, 2012.

[20] M. Otero, "Application of a continuous wave radar for human gait recognition," *Signal Processing, Sensor Fusion, and Target Recognition XIV*, 2005.

[21] Z. Xia *et al.*, "Person identification with millimeter-wave radar in realistic smart home scenarios," *IEEE Geoscience and Remote Sensing Letters*, vol. 19, pp. 1–5, 2022.

[22] V. L. Petrovic *et al.*, "High-accuracy real-time monitoring of heart rate variability using 24 ghz continuous-wave doppler radar," *IEEE Access*, vol. 7, pp. 74 721–74 733, 2019.

[23] A. B. Romeo, C. Horellou, and J. Bergh, "A wavelet add-on code for new-generation n-body simulations and data de-noising (jofiluren)," *Monthly Notices of the Royal Astronomical Society*, vol. 354, no. 4, pp. 337–344, 2004.

[24] S. M. Moghaddam *et al.*, "A self-grounded dual-polarized wideband bowtie with improved mimo performance in random-los," *2016 IEEE International Symposium on Antennas and Propagation (APSURSI)*, 2016.

[25] Y. Kim and H. Ling, "Human activity classification based on micro-doppler signatures using a support vector machine," *IEEE Transactions on Geoscience and Remote Sensing*, vol. 47, no. 5, pp. 1328–1337, 2009.

[26] J. S. Milton and J. C. Arnold, *Introduction to probability and statistics principles and applications for engineering and the Computing Sciences.* McGraw-Hill, 2003.